



Photochemical behaviour of a new 1,2,3,4-tetrahydroxanthylum fluorescent dye with “rhodamine-like” structure in liquid media and adsorbed onto a TiO₂ photo-responsive substrate



D.S. Conceição^a, D.P. Ferreira^a, Y. Prostota^b, P.F. Santos^b, L.F. Vieira Ferreira^{a,*}

^a Centro de Química-Física Molecular and IN-Institute of Nanoscience and Nanotechnology Instituto Superior Técnico, Universidade de Lisboa, Av. Rovisco Pais, 1049-001 Lisboa, Portugal

^b Centro de Química, Vila Real Universidade de Trás-os-Montes e Alto Douro, 5001-801 Vila Real, Portugal

ARTICLE INFO

Article history:

Received 25 November 2015

Received in revised form

27 January 2016

Accepted 28 January 2016

Available online xxx

Keywords:

Rhodamines

1,2,3,4-tetrahydroxanthylum

Luminescence

Titanium oxide

Radical cation

Transient absorption

ABSTRACT

A new “rhodamine-like” fluorescent NIR dye based on the 9-(2'-carboxyphenyl)-6-(*N,N*-diethylamino)-1,2,3,4-tetrahydroxanthylum system was synthesized. Its spectral-luminescent properties were investigated both in solution and adsorbed onto a TiO₂ photoactive solid substrate. Regarding liquid samples, the highest fluorescent quantum yield and fluorescence lifetime were obtained in dichloromethane ($\phi_F = 0.28$, $\tau_F = 2.67$ ns) while in ethanol and acetonitrile we observed the largest Stokes Shift, indicating a twisted intramolecular charge transfer mechanism. Additionally, the behaviour of the dye adsorbed onto TiO₂ revealed some interesting features regarding the formation of the radical derived from the dye cation, following the electron injection in the conduction band of the semiconductor. Laser flash photolysis and ground state diffuse reflectance were used to evaluate and discriminate the mechanism of photoexcitation presented, as well as to characterize the photostability of the molecule. In this case, two different scenarios could be recognized: the self-photosensitization pathway and the photocatalytic mechanism.

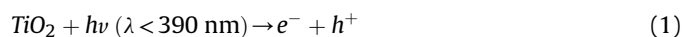
© 2016 Elsevier Ltd. All rights reserved.

1. Introduction

Rhodamine dyes are one of the most explored families of molecules regarding fluorescent applications, mostly due to their high fluorescence quantum yields, high photostability, high extinction coefficients and low intersystem crossing quantum yield. Classic rhodamines such as Rhodamine 6G, Rhodamine B and Rhodamine 101 are generally employed as laser dyes and fluorescence standards [1–5] but the demand for new rhodamine dyes is still significant, considering the extensive range of different systems in which fluorescent dyes can be applied to. For instance, near-infrared (NIR) responsive dyes with high solubility in aqueous solutions, for biological applications [6,7], and visible responsive dyes with high stability, together with an appropriate redox potential and a low quantum yield of triplet formation, in the case of photovoltaic applications, specifically, in dye sensitized solar cells (DSSCs), which are titanium oxide (TiO₂) based systems [8–11]. In

the latter case, dye-TiO₂ interactions are the primary and most important event of the device. This is due to the injection of an electron from the dye excited state into the conduction band (CB) of the TiO₂, which initiates the dye sensitization process in this kind of photovoltaic systems. The respective recombination between injected electrons and oxidized dyes, which occurs after the electron injection, is also entirely dependent on the dye-TiO₂ interactions.

The well-known photocatalytic properties of TiO₂ are derived from the formation of photogenerated charge carriers (hole and electron) which occurs upon the absorption of ultraviolet (UV) light corresponding to the band gap energy of the semiconductor. Thus, as electrons are promoted from the valence band to the conduction band, they can generate electron–hole pairs as shown in Equation (1):



Valence band (h^+) potential is positive enough to generate hydroxyl radicals (HO^\bullet) at TiO₂ surface and the conduction band (e^-)

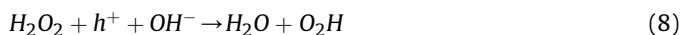
* Corresponding author.

E-mail address: LuisFilipeVF@ist.utl.pt (L.F. Vieira Ferreira).

potential is negative enough to reduce molecular oxygen into superoxide ion radical ($O_2^{\cdot-}$) – Equations (2) and (3), respectively.



These radicals will participate in the degradation of the dye. However, two different mechanisms can be mentioned regarding the dye–TiO₂ interaction and the consequent formation of radicals such as HO[•], O₂^{•-}, hydroxylated intermediates and the dye radical cation. As already well stated in the literature [12,13], these two pathways can be defined as the photocatalytic mechanism, and the self-photosensitized pathway, depending of the excitation source, UV irradiation or visible light illumination, respectively. One of the intermediates formed in these reactions is H₂O₂, which is also photoactive and can be split in HO[•] and OH⁻ after irradiation [14,15].



Therefore, it can be used as an electron scavenger, to mimic some of the effects presented in the dye–TiO₂ system, namely the possible formation of a radical cation.

The technique of laser flash photolysis has been extensively addressed in the past to characterized TiO₂ based materials, in what concerns the kinetics of the electron–hole separation and recombination [16–18]. In this way, it is possible to identify, until several nanoseconds after laser excitation, the trapped electron and the trapped hole, at the surface of the semiconductor. Following that, it is also expected and possible to obtain, by means of this technique, data that supports the interaction of the dye with the semiconductor and the intermediates formed after irradiation.

It is assumed from previous studies regarding rhodamines and rhodamine-like molecules that the molecular structure and nature of the solvent play an important role in the mechanisms that control the fluorescence yields of rhodamine dyes. Specifically, it was found that deactivation mechanisms of the first excited singlet state involving intramolecular charge transfer (ICT) interactions were directly correlated with structural modifications that enabled a larger Stokes shift [19,20]. Taking all these features into account, a new dye (7) derived from the 9-(2'-carboxyphenyl)-6-(N,N-diethylamino)-1,2,3,4-tetrahydroxanthylum system possessing a "rhodamine-like" structure was synthesized (Scheme 1) and was characterized in terms of its behaviour in liquid and solid samples. In the first case, three different solvents were used – dichloromethane, ethanol and acetonitrile – and a complete photochemical evaluation was performed. In solid samples, the main goal was to study the behaviour of the dye adsorbed onto a photoactive material such as TiO₂, in the presence of light. Cellulose was used as the inert standard material, for comparison purposes. The scope of this work targets a better understanding of the mechanisms involved in the photochemical behaviour of this new synthesized dye, in substantially different environments.

2. Experimental section

2.1. General

Titanium (IV) oxide (nanopowder, <25 nm particle size) was obtained from Sigma–Aldrich and microcrystalline cellulose (powder) was obtained from Fluka. Solvents used in the measurement of spectral-luminescent properties were of spectroscopic grade. Reagents and solvents used in the synthesis of the dye were of commercial origin and, unless otherwise stated, used as received. All reactions were monitored by thin-layer chromatography on aluminium plates pre-coated with Merck silica gel 60 F254 (0.25 mm). 9-(2'-carboxyphenyl)-6-(N,N-diethylamino)-1,2,3,4-tetrahydroxanthylum perchlorate (3) [25] and 3-methylimidazo[1,5-a]pyridine (5) [26] were prepared as previously described. ¹H and ¹³C NMR spectra were recorded on a Bruker ARX400 spectrometer (at 400.13 and 100.62 MHz, respectively); δ in ppm relative to residual solvent signals and J in Hz. IR spectra were obtained on a Unicam Research Series FT-IR spectrometer; ν_{max} in cm⁻¹. High resolution electrospray ionization time-of-flight (ESI-TOF) mass spectra were measured with a VG AutoSpec M spectrometer. Melting points were determined in open capillary tubes in a Buchi 535 melting point apparatus and are uncorrected.

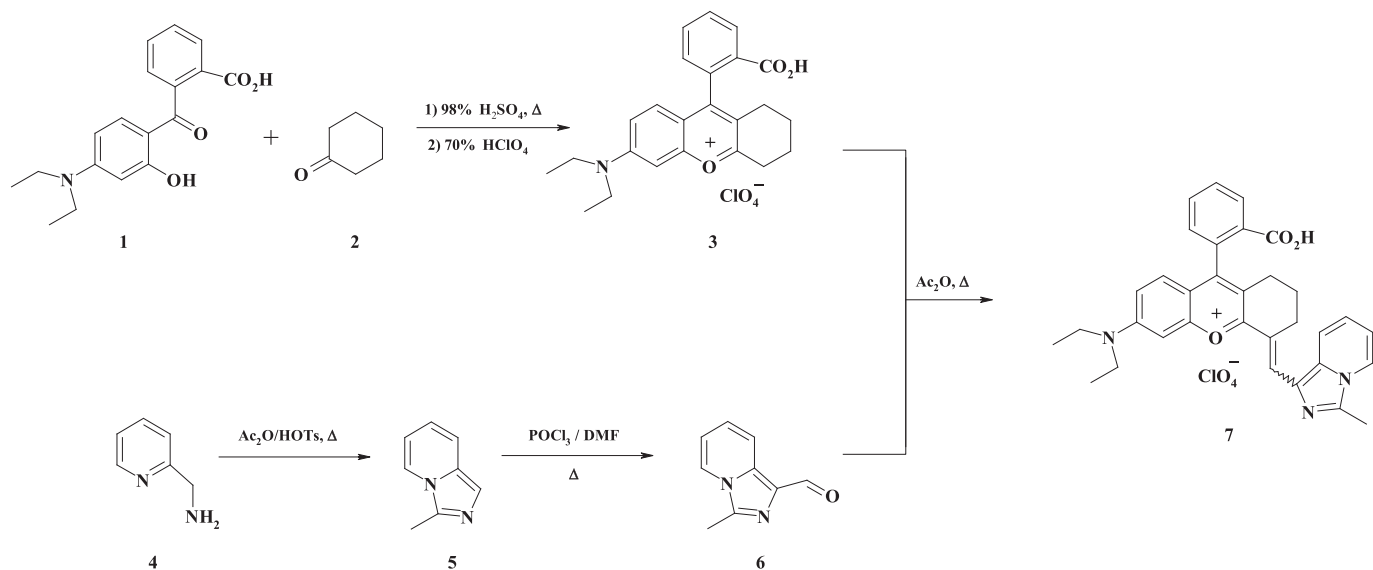
2.2. Synthesis of the dye

2.2.1. 3-Methylimidazo[1,5-a]pyridine-1-carbaldehyde (6)

To a solution of 3-methylimidazo[1,5-a]pyridine (5) (1.50 g, 11.4 mmol) in anhydrous dimethylformamide (10 mL), under vigorous stirring at 0–5 °C, was added dropwise freshly distilled phosphorus oxychloride (1.10 mL, 11.8 mmol) during 30 min. Once the addition was complete, the reaction mixture was kept at room temperature for 30 min, and then heated to 100 °C for additional 3 h. After cooling to room temperature, the reaction mixture was poured into water (100 mL) and made alkaline with 20% aqueous sodium hydroxide. The resulting mixture was extracted with dichloromethane (3 × 20 mL), washed with water (50 mL), dried over anhydrous sodium sulfate and evaporated to dryness under reduced pressure. The resulting solid residue was recrystallized from propan-2-ol to afford 2 (1.30 g, 71%) as yellow flakes. Mp 132–134 °C. IR (KBr) ν_{max}: 755, 830, 1027, 1295, 1484, 1640, 1871, 2773. ¹H NMR (CDCl₃, 298 K) δ: 2.66 (3H, s), 6.88 (1H, t, J = 6.7), 7.18 (1H, t, J = 7.8), 7.85 (1H, d, J = 6.9), 8.18 (1H, d, J = 8.9), 10.00 (1H, s). ¹³C NMR (CDCl₃, 298 K) δ: 12.5, 115.1, 119.4, 121.8, 125.7, 129.2, 133.9, 137.2, 185.1. HRMS (ESI-TOF) m/z: 160.06391 (M⁺; calc. for C₉H₈N₂O: 160.06374).

2.2.2. 9-(2'-carboxyphenyl)-6-(N,N-diethylamino)-4-[(3-methylimidazo[1,5-a]pyridin-1-yl)methylidanyl]-1,2,3,4-tetrahydroxanthylum perchlorate (7)

A solution of 2 (0.07 g, 0.43 mmol) and 3 (0.20 g, 0.42 mmol) in freshly distilled acetic anhydride (5 mL) was heated under reflux for 5 min. The reaction mixture was cooled to room temperature and the residue formed was filtered off, and washed with ethyl acetate (10 mL) and diethyl ether (5 mL) to afford chromatographically pure 4 (0.17 g, 65%) as a green solid with metallic lustre. Mp 246–248 °C (dec.). IR (KBr) ν_{max}: 706, 754, 841, 1059, 1176, 1254, 1319, 1437, 1532, 1581, 1628, 1729. ¹H NMR (DMSO-d₆, 323 K) δ: 1.26 (6H, t, J = 7.0), 1.73–1.76 (2H, m), 2.28–2.37 (2H, m), 2.75 (3H, s), 3.34–3.43 (2H, m), 3.64 (4H, q, J = 7.0), 6.86 (1H, d, J = 9.4), 7.09 (1H, dd, J = 2.4, 9.4), 7.17 (1H, t, J = 6.8), 7.30 (1H, d, J = 2.4), 7.38 (1H, d, J = 7.5), 7.49 (1H, m), 7.74 (1H, t, J = 7.4), 7.84 (1H, t, J = 7.5), 8.19 (1H, d, J = 7.4), 8.42–8.48 (3H, m). ¹³C NMR (DMSO-d₆, 298 K) δ: 12.5, 20.5, 20.9, 25.9, 26.5, 44.8, 95.7, 114.8, 115.4, 155.7, 118.0, 119.9, 121.1, 124.9, 126.5, 127.3, 128.6, 129.0, 129.7, 129.8, 130.8,



Scheme 1. Synthesis of dye 7.

132.9, 134.6, 137.8, 141.6, 153.5, 156.8, 163.6, 166.4, 171.9. HRMS (ESI-TOF) m/z : 518.24278 (M^+ ; calc. for $C_{33}H_{32}N_3O_3$: 518.24381).

2.3. Sample preparation

Liquid samples were prepared by diluting the dye in the three solvents used in this work: acetonitrile, chloroform and dichloromethane. The optical density was adjusted to 0.6, in all cases. Solid samples were prepared by solvent evaporation under constant stirring, followed by an overnight vacuum drying cycle. In that case, a solution of the dye in acetonitrile was used, with a concentration of 1.0×10^{-4} M, followed by its adsorption on 200 mg of solid substrate. Then, the solvent was allowed to evaporate until the powder remained on the flask. For solid samples, concerning TiO_2 , all steps were prepared in the dark, to avoid immediate dye degradation. TiO_2 dispersions in acetonitrile solutions of the dye were prepared with a dye concentration of 1.0×10^{-4} M, mixing 40 mg of TiO_2 in 4 mL of solution.

2.4. UV–visible absorption spectra and ground state diffuse reflectance spectra (GSDR)

Steady-state absorption spectra were recorded with the use of a CamSpec M501 single beam scanning UV/Visible spectrophotometer at room temperature in the spectral range from 190 to 1100 nm. The optical densities were measured using a UV quartz cuvette (1 cm path length). Ground-state absorption studies were performed using a homemade diffuse reflectance laser flash photolysis setup, with a powerful 150 W tungsten-halogen lamp as monitoring lamp, triggering the system in the normal way but without the laser fire, and in this way recording the lamp profile for all samples under study and also for two standards, barium sulfate and magnesium oxide powders. A fixed monochromator coupled to an ICCD with time gate capabilities was used for detecting the reflectance signals. The reflectance, R , from each sample was obtained in the UV–Vis–NIR spectral regions and the remission function, $F(R)$, was calculated using the Kubelka–Munk equation for optically thick samples. The remission function is $F(R) = (1 - R)^2/2R$. Details regarding the data treatment can be found in Ref. [21] and references quoted therein. For the photocatalytic evaluation of the dye onto TiO_2 , the GSDR spectra were

recorded continuously in specific time intervals: 1 min, 5 min, 10 min, 20 min, 30 min, 40 min, 50 min and 60 min.

2.5. Laser-induced luminescence (LIL): fluorescence emission quantum yield determinations

Schematic diagrams of the LIL system are also presented in Ref. [21]. A N_2 laser (PTI model 2000, ca. 600 ps of full width at half maximum (FWHM), ~ 1.0 mJ per pulse, 5 Hz), was used in the laser-induced luminescence experiments, the excitation wavelength being 337 nm for the liquid samples. In that case, the optical density at the excitation wavelength (337 nm from the N_2 laser) used for both the unknown and standard samples was 0.6, following the methodology of a previous publication [22]. In our set-up the errors in the determination of ϕ_F are $\pm 3\%$. The fluorescence quantum yields of dye 7 in acetonitrile, chloroform and dichloromethane were calculated relative to the standard from their respective average fluorescence peak areas, and the published quantum yield of the standard, which in this case was Rhodamine 101 ($\phi_F = 0.98$ in ethanol). For solid samples, in the case of the dye's adsorption onto TiO_2 , its fluorescence emission was acquired by means of laser excitation at 500 nm, and by using a cut-off filter of 590 nm, together with an optical density filter of 2.2%.

2.6. Fluorescence lifetimes determination

Fluorescence lifetimes were determined, in the case of liquid samples, using EasyLife V™ equipment from OBB (Lifetime range from 90 ps to 3 ms). This technique uses pulsed light sources from different LEDs (630 nm in this case) and measures fluorescence intensity at different time delays after the excitation pulse. In this case a 695 nm cut-off filter was used. The instrument response function was measured using a Ludox scattering solution. FelixGX software from OBB was used for fitting and analysis of the decay dynamics.

2.7. Laser flash photolysis: triplet–triplet transient absorption spectra

The schematic diagrams for the laser flash photolysis technique and the used methodology are presented in Refs. [21,23,24]. For the

laser flash spectra shown, the fourth harmonic of a Nd:YAG laser (266 nm, ca. 6 ns full-width half maximum, FWHM) from B. M. Industries (Thomson-CSF, model Saga 12-10, France) was used, by employing the transmission mode, in the case of liquid samples, and reflectance mode, in the case of solid substrates. In the first case, the monitoring lamp used was a 150 W quartz tungsten-halogen in an Oriel housing, whereas in the latter case a 450 W xenon lamp was applied to the geometry. The light arising from the irradiation of the samples by the laser pulse, with approximately 60 mJ per pulse, was collected by a collimating beam probe coupled to an optical fibre (fused silica) and detected by a gated intensified charge coupled device Oriel model Instaspec V, (Andor ICCD, based on the Hamamatsu S57 69-0907). The ICCD was coupled to a fixed compact imaging spectrograph (Oriel, model FICS 77441). The system can be used either by capturing all light emitted by the sample or in a time-resolved mode by using a delay box (Stanford Research Systems, model D6535), whenever needed. The ICCD has high speed gating electronics (about 2.3 ns) and intensifier, covering at least the 250–900 nm wavelength range. Liquid samples were prepared with an optical density of 0.9 at the excitation wavelength, and oxygen removal was achieved by argon bubbling for about 15 min. Transient absorption data are reported as change of optical density ΔOD or percentage of absorption defined by % Abs = $100 \Delta J_t / J_0 = 100 (1 - J_t / J_0)$, where J_0 and J_t are the transmitted light from sample before exposure to the exciting laser pulse and at time t after excitation, respectively.

3. Results and discussion

3.1. Synthesis

The target “rhodamine-like” dye 7 was synthesized in good yield via simple condensation of 9-(2'-carboxyphenyl)-6-(*N,N*-diethylamino)-1,2,3,4-tetrahydroxanthylum perchlorate (2) with 3-methylimidazo[1,5-*a*]pyridine-1-carbaldehyde (5), in acetic anhydride (Scheme 1). The synthesis of the starting 1,2,3,4-tetrahydroxanthylum salt 3 was carried out by an improved method developed by one of us involving the cyclocondensation of 2-[4-(*N,N*-diethylamino)-2-hydroxybenzoyl]benzoic acid (1) with cyclohexanone (2) [25]. Aldehyde 6 was obtained through Vilsmeier–Haack formylation of 3-methylimidazo[1,5-*a*]pyridine (5), readily prepared by cyclocondensation of commercially available 2-picolyamine (4) with acetic anhydride, in the presence of an equimolar amount of *p*-toluenesulfonic acid monohydrate [26].

3.2. Ground state UV–visible spectra of dye 7, in solution

The absorption profile of the dye studied in this work, in three different solvents, acetonitrile, ethanol and dichloromethane, is presented in Fig. 1. It is well established that the solvatochromic behaviour of rhodamine dyes and their derivatives arise from different types and extent of solute and solvent interactions in the solution media. These interactions mainly include non-specific (dielectric enrichment) or specific interactions, such as hydrogen bonding, proton transfer, and intermolecular charge transfer (ICT). In fact, there are competition mechanisms between the solute–solute and solute–solvent interactions that determine the nature of solvatochromic behaviour of the solute molecules [27,28]. When compared with the classic Rhodamine B, it can immediately be seen the large bathochromic deviation of the absorption maxima, which can imply the importance of the fused imidazole-pyridine rings in the increase of the resonance of the molecule (typically, the absorption maxima of rhodamine B is approximately 543 nm, depending on the solvent).

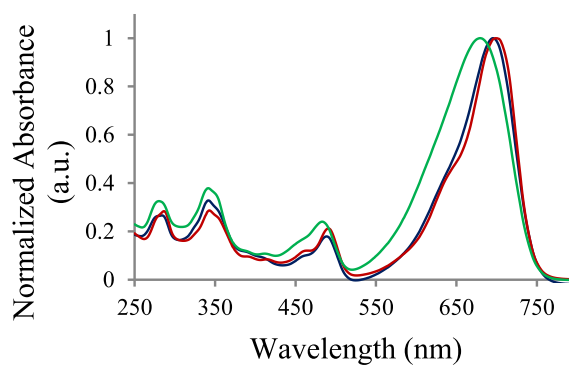


Fig. 1. Absorption spectra of dye 7 in acetonitrile (blue), dichloromethane (red), and ethanol (green). (For interpretation of the references to colour in this figure legend, the reader is referred to the web version of this article.)

Ethanol and acetonitrile are the more polar solvents, with Dimroth's ET and Kosower's Z solvent parameters of 51.9 and 79.6, in the case of ethanol and 46 and 71.3, in the case of acetonitrile. Dichloromethane possesses an ET parameter of 41.1 and a Z-value of 64.2 and within the scope of this work, it is the solvent with the lowest polarity. The solvent polarity parameters can be directly correlated to Stokes shift (the shift between the ground state and excited state transitions of dyes), i.e. the large Stokes shift is also indicative of the charge transfer transition. The large magnitude of the Stokes shift indicates that the excited state geometry could be different from that of the ground state. Generally speaking, increments in the Stokes shift value are a function of an increase in solvent polarity, which indicates an increase in the dipole moment of the excited state. In such cases, the relaxed excited singlet-state (S_1) will be energetically stabilized compared to the ground state (S_0) and a significant red shift of fluorescence will be observed. The Stokes Shift values will be presented and discussed in the following section. The absorption bands of the dye in both acetonitrile and dichloromethane are red-shifted, compared to the most polar solvent, ethanol. This evidences that the observed λ_{max} is, as expected for this type of molecules, a complex function of both polarity and polarisability of the solvent. The same behaviour is also witnessed for the fluorescence emission'. This trend is in accordance with the solvatochromic behaviour of rhodamine B and rhodamine 6G, already studied and reported in the literature [27]. Thus, it can be expected that the solvent polarity features present the main contribution in solvatochromism of rhodamine and rhodamine-like dyes.

3.3. Fluorescence emission spectra and fluorescence lifetime decays

The laser induced fluorescence emission of dye 7 in the three solvents studied in this work is presented in Fig. 2. The spectra show a significant emission in the range of 650–900 nm, presenting a huge displacement when compared with the classical rhodamine B (with maxima at approximately 560–575 nm, depending on the solvent). This deviation is indeed higher than the one observed in the absorption bands, pointing out to the occurrence of intramolecular charge transfer mechanisms of deactivation of the excited state. This feature is also complementary to the large Stokes shift that is usually present in dyes that exhibit this behaviour.

Table 1 presents the most important parameters obtained for the dye under study. Together with internal conversion and intersystem crossing deactivation pathways, ICT can also play an important role in the deactivation of the lowest singlet state, contributing to the reduction of the quantum yield for the

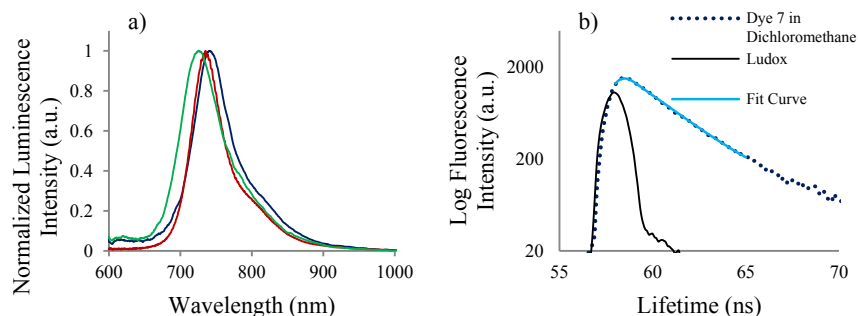


Fig. 2. a) Fluorescence emission spectra of dye 7 in acetonitrile (blue), dichloromethane (red) and ethanol (green). b) Fluorescence decay curve, instrument responsive curve (IR), and fitting of the dye, in dichloromethane. (For interpretation of the references to colour in this figure legend, the reader is referred to the web version of this article.)

Table 1
Spectral data of dye 7 in acetonitrile, dichloromethane and ethanol.

	λ_{abs} (nm)	λ_{emi} (nm)	ϕ_F	τ_F (ns)	k_F	Stokes shift (nm)
CH ₃ CN	695	741	0.16	1.67	1.0×10^8	46
CH ₂ Cl ₂	699	735	0.28	2.67	1.1×10^8	36
EtOH	680	725	0.20	1.98	1.0×10^8	45

fluorescence emission, ϕ_F , and for the increase of the rate constant associated with the non-radiative path of deactivation. This effect is more significant in polar solvents, and, indeed, that seems to be the case, when analyzing the fluorescence quantum yields and fluorescence lifetimes. Dichloromethane exhibits the highest value of ϕ_F and τ_F , 0.28 and 1.98 ns, respectively. Its fluorescence lifetime profile is also shown in Fig. 2. In acetonitrile, the lowest values of fluorescence quantum yield and fluorescence lifetime were obtained, 0.16 and 1.67 ns, respectively.

3.4. Transient absorption analysis

The transient absorption measurements, obtained by means of laser flash photolysis in transmittance mode, enables the monitoring of transient species that can be formed after laser excitation. In this case, the dye was excited at 266 nm, in acetonitrile. Acetonitrile was selected as the solvent of use due to the lower fluorescence emission of the dye in it, and because the solid samples (cellulose and TiO₂ substrates) were also prepared with this solvent. It is well known that titanol groups act as surface traps for the photogenerated hole, preventing the recombination rate and, theoretically, increasing the photo-activity of the semiconductor [29]. These titanol groups are created from the residual water that exists at the surface. Every solvent has a residual content of water, and therefore, to minimize this effect at the solvent evaporation step, acetonitrile was the solvent of choice since it is the one with the smallest amount of water, when compared with ethanol and dichloromethane (Acetonitrile: 0.007%; Ethanol – 0.2%; Dichloromethane – 0.02%). Fig. 3 displays the results obtained by this technique in an argon purged sample with an acquisition gate width of 2 μ s, and immediately after the laser pulse. The spectrum show two important features: the first one is the ground state depletion, which assumes negative values since it is the initial species presented in the sample, before excitation. The minimum for the depletion is located at approximately 695 nm, equivalently to the UV–visible absorption spectra presented previously. In addition to that, the minima peaking at approximately 490 nm and 330 nm can also be identified, Dye_{depl}, with lower intensities, when compared with the main depletion; the second important feature is the triplet–triplet absorption band, ³Dye*, located between 300 and 585 nm, only interrupted by the two small depletions of the

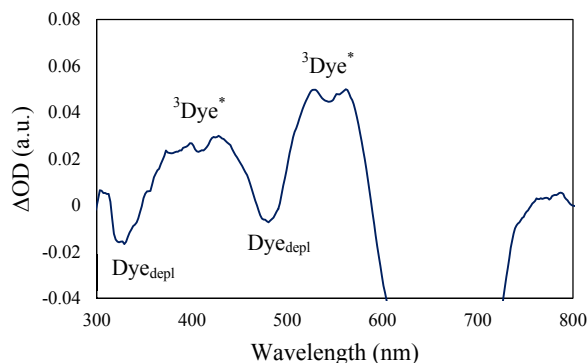


Fig. 3. Transient absorption spectrum of dye 7, in acetonitrile, in an argon purged sample.

dye molecule, previously mentioned. The same pattern, of triplet–triplet absorption and ground state depletion is already well established in the literature, for instance in the cases of rhodamine 101, rhodamine 6G, rhodamine 3G and sulforhodamines 101 and B [30,31]. No significant information was observed for air equilibrated samples.

3.5. Ground state diffuse reflectance (GSDR) spectra of dye 7, adsorbed onto cellulose and TiO₂

The GSDR spectra of the dye 7 were initially obtained in cellulose, the inert substrate. Samples of the dye adsorbed onto microcrystalline cellulose were prepared with five different concentrations, as depicted in Fig. 4. The first spectra shown (Fig. 4 – Top) are quite similar to the one obtained in solution, with a rather well defined vibronic structure, for all five concentrations, and a maximum absorption wavelength peaking at 680 nm. A crucial characteristic for efficient dyes, used in photochemical applications such as photovoltaic devices, is the presence of suitable functional groups in their structure which can strongly bind to the surface of semiconducting metal oxides. It is well known that when considering mainly covalent attachment brought about by directly linking groups of interest or via linking agents, groups such as silanyl, amide, carboxyl and phosphonate have been shown to form stable linkages. In this case, the anchoring group of the molecule, which reacted with surface hydroxyl groups of the metal oxide surface – titanol groups – is the carboxylic acid. Compared with cellulose, the spectra of the dye adsorbed onto TiO₂ nanopowder (Fig. 4 – bottom), is completely different. Besides the typical UV absorption band of TiO₂ with maximum at approximately 350 nm, the plot shows that the vibronic definition of the dye is absent, for the five concentrations used. The effect is most probably due to the

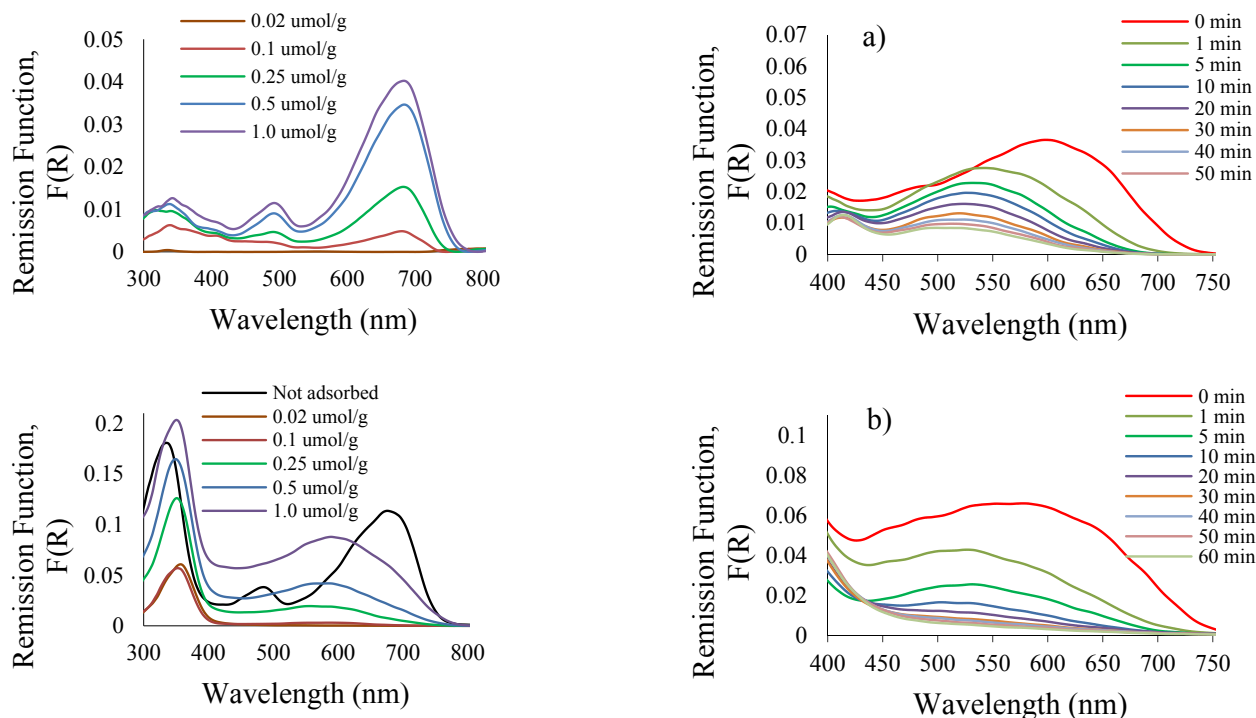


Fig. 4. GSDR spectra of dye 7 adsorbed onto Cellulose (Top) and TiO_2 (Bottom).

immediate interaction of the dye- TiO_2 system with the light from the excitation lamp (inherent to the technique of GSDR). In that case, the dye radical cation is instantly formed, leading to the loss of conjugation by the molecule and, consequently, the disappearance of its previously well defined absorption bands, with a shift to lower wavelengths. Following that, only a single absorption band could be detected, peaking at approximately 590 nm. On the other hand, in the case of a fresh TiO_2 dispersion in a solution of the dye, the immediate monitoring of the GSDR depicts the same absorption profile found in cellulose, apart from the typical TiO_2 absorption peaking on the UV range. Within the range of concentrations presented, the sample of 0.5 $\mu\text{mol/g}$ was chosen as the best one to perform the remaining photochemical characterization, without attaining aggregation phenomena. To confirm that, the fluorescence emission of the dye adsorbed onto cellulose using all five concentrations was monitored. The maximum fluorescence emission intensity was obtained for the concentration of 0.5 $\mu\text{mol/g}$ (data not shown).

3.6. Photocatalytic degradation of the dye

The photocatalytic degradation of dye 7, adsorbed onto TiO_2 , was monitored, as mentioned in the experimental section, by means of a 150 W tungsten-halogen lamp, which constantly irradiated the sample, for 60 min. As already stated in the introductory section of this work, two different mechanisms and pathways can be presented in this types of systems, where an organic dye is adsorbed onto TiO_2 . Depending if the excitation source is targeting directly the dye or the semiconductor, different kinetics can be obtained for the degradation of the molecule, as presented in Fig. 5. Fig. 5a) shows the $F(R)$ function of the sample prepared with a concentration of 0.5 $\mu\text{mol/g}$, monitored for 60 min of lamp exposure, with no cut-off filters. The lamp irradiation profile applies in the range of approximately 250–1000 nm, and this feature means that within this range of wavelengths, both the semiconductor and the dye are

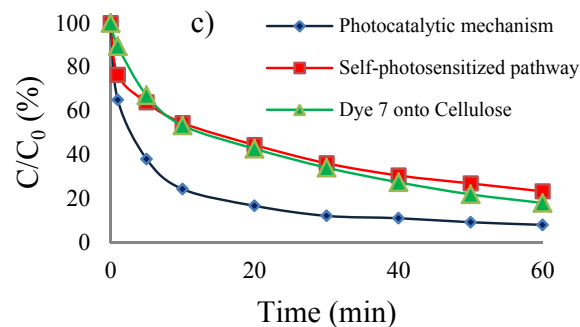
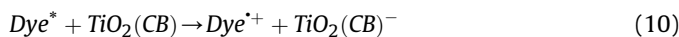


Fig. 5. Photodegradation of dye 7, adsorbed onto TiO_2 . a) Photocatalytic mechanism + Self-photosensitized pathway; b) Self-photosensitized pathway; c) Degradation kinetics, including the photodegradation effect of the Xe lamp, on a dye – Cellulose sample.

being excited, enabling both the photocatalytic mechanism and the self-photosensitized pathway. The plot shows that, as stated before, only the band peaking at approximately 590 nm can be seen. However, after approximately 1 min of exposure, a hypsochromic shift can be observed, of approximately 65 nm (to ~ 525 nm). This effect was surely due to the presence of another neo-formed species. Regarding Fig. 5b), it presents the dye photodegradation profile when enabling only the self-photosensitized pathway. For that purpose, a cut-off filter of 414 nm was used, therefore preventing the direct excitation of the TiO_2 substrate. In general, the features presented by Fig. 5a and b could mean that, almost immediately after light absorption, the dye could be promoted to its excited state and would transfer an electron to the conduction band of the semiconductor leading to the formation of the dye radical cation, as suggested by Equations (9) and (10). Therefore, the first curve of both spectra ($t = 0$) trades the initial contact between the sample and the excitation light, in which there is still some ground state absorption profile from the original state of the dye, balanced

with the instantly generation of the radical cation. The proposed mechanism is further explored in this section.

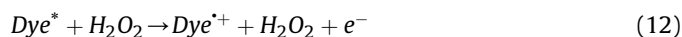


The kinetics of the photodegradation effect of the TiO_2 , following both the photocatalytic mechanism and the self-photosensitized pathway, and only the latter one, on the dye, is evidenced in Fig. 5c). In the first case, after 60 min, only 8% of the molecules were still intact at the surface of TiO_2 , showing the strong photocatalytic capability of the semiconductor. Following this pathway and after the generation of the electron–hole pair there is a significant production of radical species that degrade the molecule, either at the valence band with the production of OH radicals from the adsorbed H_2O at the surface of TiO_2 , or at the conduction band, yielding $\text{O}_2^{\cdot-}$, which participate in the production of HO^{\cdot} , H_2O_2 and, ultimately, HO^{\cdot} . However, the dye would also present a significant photodegradation after being exposed to the lamp. Therefore, to evidence the photodegradation capability of TiO_2 on this molecule, this study was also performed with dye 7 adsorbed onto cellulose. The results showed that there is a 3-fold increase in the photocatalytic capability of the system when using TiO_2 , compared with the inert substrate.

To understand the nature of the new species, formed almost immediately after irradiation, onto TiO_2 , a different strategy was employed, by dispersing the commercial TiO_2 nanopowder in a dye solution (1.0×10^{-4} M), in acetonitrile, and using a powerful 450 W Xe lamp. A key point of the strategy was that the output of the lamp was cut off below 414 nm, by means of a cut-off filter. In this way, only the self-photosensitized pathway would be privileged and excessive photodegradation prevented. For reaching a faster and better understanding of the behaviour of the dye in the presence of TiO_2 , the monitoring of the GSDR and luminescence spectra of the dispersion was performed. After lamp excitation for approximately 2 min, the dispersion was continuously stirred until reaching an acceptable degree of homogeneity. The obtained results are presented in Fig. 6a). Regarding the GSDR, it shows three important features: the characteristic absorption band of TiO_2 , in the 240–400 nm range, a first absorption peaking at approximately 525–530 nm, attributed to the dye radical cation, $\text{Dye}^{\cdot+}$, and another absorption with a maximum located at 655 nm, attributed to the original absorption of the dye, already deviated from its initial absorption maximum, presumably due to the immediate formation of the radical cation. Despite that fact, the same hypsochromic shift previously observed (–65 nm) remains, showing that the mechanism underlined here is most probably an electron

transfer from the dye to the TiO_2 material. In what concerns the luminescence spectrum, the same dual-band profile remains, with a maximum at around 735 nm, relative to the fluorescence emission of the dye, and another located at approximately 600 nm, concerning the radical cation, $\text{Dye}^{\cdot+}$. The absorption and emission band placed at 655 nm and 735 nm, respectively, that endured minutes of lamp excitation and stirring, are certainly related not only with the molecules that did not undergo through electron transfer processes but also with the molecules in the dispersion that were not adsorbed onto the powdered TiO_2 material. The macroscopic behaviour of the dispersion is illustrated in Fig. 6b). Immediately after lamp excitation (a few seconds), the pattern is the one presented: a violet color starts to appear from the top of the flask, towards the semiconductor powder, implying that the dye is transferring and injecting e[–] to the TiO_2 material.

To properly ensure that this phenomena is due to electron transfer, and that, possibly, the radical cation is formed, a solution of the dye of interest, in acetonitrile, together with hydrogen peroxide (H_2O_2 , 1:5 v/v), was prepared, and submitted to lamp irradiation. It is well known and it was already mentioned in the introductory section of this work that H_2O_2 can trap the photoinduced e[–] originated from TiO_2 to stabilize the paired e[–]-h⁺ [14]. In a similar way, H_2O_2 can also accept an electron from the dye, originating not only the dye's radical cation, but HO^{\cdot} . In addition to that, the photodissociation of H_2O_2 also creates additional HO^{\cdot} . These mechanisms can be defined by the following equations:



Adding to the already presented Equation (7),



and finally,



Ultimately, the interaction of the dye with H_2O_2 will result in the dye's radical cation and hydroxylated intermediates which, at the end, will contribute for the degraded products of the original dye:

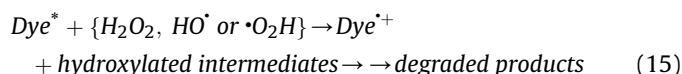


Fig. 7 validates the assumptions presented in this work, regarding the formation of the radical cation, since it displays a new band arising at approximately 540 nm after photoexcitation and in

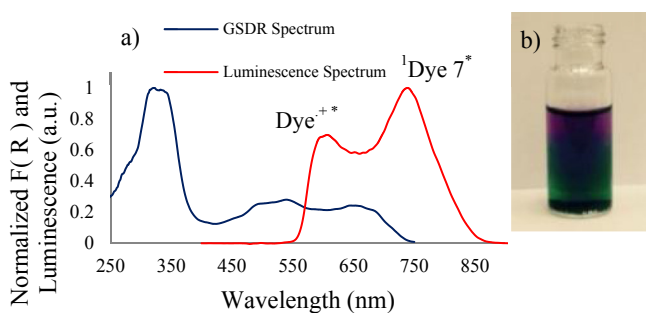


Fig. 6. a) GSDR and Luminescence spectrum of a previously excited TiO_2 dispersion, in a dye solution, by means of a Xe lamp. b) Macroscopic behavior of the dispersion, after a few seconds of excitation.

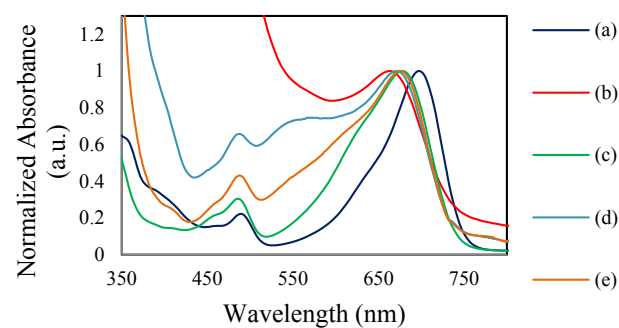


Fig. 7. Absorption spectra of (a) dye 7 in CH_3CN , (b) Photodegradation of the dye in acetonitrile, (c) The dye in $\text{CH}_3\text{CN}:\text{H}_2\text{O}_2$ (5:1 v/v), (d) Photodegradation of the dye in $\text{CH}_3\text{CN}:\text{H}_2\text{O}_2$ (5:1 v/v) after 5 min of excitation, (e) Dark recovery.

the presence of H₂O₂ (d). Besides that fact, this new band can also be qualified as reversible, since it disappears in the dark (e). This is consistent with an excitation/deexcitation mechanism which corroborates the sensitization behaviour of the dye, in the presence or absence of light, respectively.

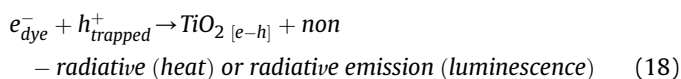
3.7. Laser flash photolysis applied to the system dye-TiO₂

Laser flash photolysis has been an important tool to study the excited state carriers originated from the TiO₂ semiconductor. In the literature, several reports point out to the presence of the excited charge carrier species [32–34], namely trapped holes and trapped electrons, which would absorb light at around 500 nm and 700 nm, respectively. These species would also be generated according with the interfacial photochemical reactions described below. From photoexcitation, mentioned earlier on equation (1), it follows:



In the presence of an electron donor, such as the dye studied in this work, the following reaction can occur:

Electron-hole recombination:



The equation shows the electron–hole recombination that can occur between the electron donated by compound 7, and the hole entrapped by surficial defects such as titanol groups, commonly found at the semiconductor surface. That recombination generates the initial unexcited TiO₂ state, via non-radiative pathway (with heat emission), or via radiative pathways (luminescence emission).

Fig. 8 shows the transient absorption spectra, in reflectance mode, of the commercial TiO₂ nanopowder, and of a dye-TiO₂ sample (0.5 μmol/g). The plot shows three distinct features: a first absorption located at approximately 380 nm, which could be attributed to a deviation of the band edge of TiO₂ following the laser excitation, due to a rapid photoinduced thermal phenomenon, TiO₂^{th-depl}. The trend was already observed in the past by Wilkinson and Willsher [35], where the transient absorption spectrum was red shifted from the ground state absorption edge of TiO₂, in the case of an anatase powder; the second important signal is

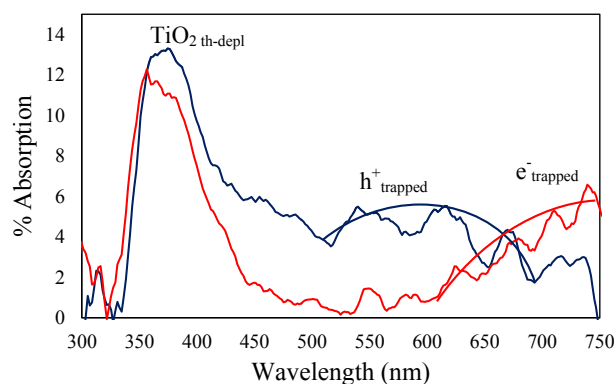


Fig. 8. Transient absorption spectra of commercial TiO₂ nanopowder (blue) and dye 7-TiO₂ sample, $c = 0.5 \mu\text{mol/g}$ (red), excited at 266 nm. Both spectra were obtained immediately after laser pulse. (For interpretation of the references to colour in this figure legend, the reader is referred to the web version of this article.)

presented in the commercial nanopowder, and locates in the 450–750 nm range. This could be attributed to the generated holes entrapped at the surface of TiO₂, h^{+}_{trapped} . This effect is directly related to the fact that the dye-TiO₂ sample does not possess this type of feature. Instead, a significant band ascends in the range of 600–750 nm. It was already mentioned that the molecule donates an electron after photoexcitation, when adsorbed onto TiO₂. Therefore, the trend suggests that the electrons donated by the molecules adsorbed onto the semiconductor surface will recombine with the superficial trapped holes, leading to the disappearance of their featuring band and to the significant grow of the characteristic band of the trapped electrons, e^{-}_{trapped} , which, as stated before, is located in the 700–800 nm range.

The powdered dye-TiO₂ system did not allow a complete evaluation of the behaviour of the dye in this environment, by means of laser flash photolysis, probably due to the thermal effect observed before, which instantly degrades the sample. Therefore, colloidal dispersions of TiO₂ in acetonitrile solutions of the dye were prepared and studied, in transmittance mode. Fig. 9 shows the transient absorption spectra of the regular, deaerated dye solution, in acetonitrile, and of a colloidal dispersion of TiO₂ in that same solution, without stirring, and in an air equilibrated environment. The assay was immediately performed after adding TiO₂ in the solution of the dye, to prevent significant dye adsorption and consequent generation of the dye radical cation. In a prepared solution of the dye, the normal pattern, previously presented, was obtained. However, for the colloidal dispersion, some interesting features were observed, starting from the fact that the triplet–triplet absorption band could be easily visible, in the same range as the one presented in solution – from 300 to approximately 585 nm. Surprisingly, this band was obtained in an air equilibrated sample, and was equivalent to the signal obtained in an argon purged sample (data not shown). Thus, the results suggest that, in the presence of TiO₂, there could be oxygen consumption from the semiconductor, which enables the triplet–triplet absorption monitoring. As previously stated, at the conduction band of the semiconductor, the oxygen presented in the neighbouring environment is consumed to generate the anion superoxide radical O_2^{-} (Equation (3)). As opposed to the trend observed on the TiO₂ nanopowder, with a reflectance geometry, no thermal photoinduced effect could be seen in the case of TiO₂ dispersions. Following that, an air equilibrated colloidal dispersion of TiO₂ in a dye's solution was prepared and photoexcited, by means of a 450 W Xe lamp, to generate the radical cation of the dye. After obtaining a homogeneous pink

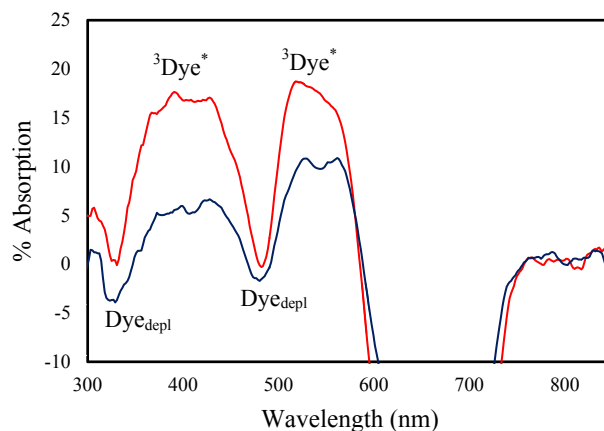


Fig. 9. Transient absorption spectra of dye 7 in acetonitrile (blue), and of TiO₂ dispersion in dye's solution (red). (For interpretation of the references to colour in this figure legend, the reader is referred to the web version of this article.)

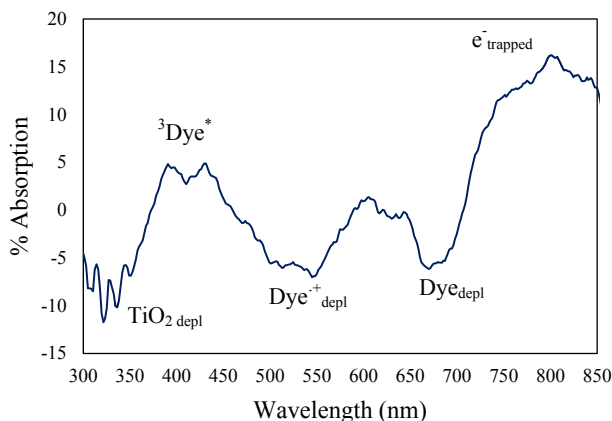


Fig. 10. Transient absorption spectra of a previously irradiated TiO_2 dispersion in a dye solution.

colloidal dispersion, the sample was monitored by laser flash photolysis, in reflectance mode, with constant stirring. The obtained transient absorption spectrum is presented in Fig. 10. In this case, the ground state depletion of the original dye and also of the radical cation can be observed, at 685 nm and 525 nm respectively. Adding to that, the same featuring pattern of the trapped electron is presented, again in the range of 700–850 nm. The triplet–triplet absorption band can also be visible, at around 430 nm, together with the usual TiO_2 ground state depletion, peaking at approximately 330 nm. All the characteristic features of the original dye presented in this spectrum reflect the molecules from the dispersion that did not completely adsorb onto the TiO_2 .

4. Conclusions

In this report a new 9-(2'-carboxyphenyl)-1,2,3,4-tetrahydroxanthylum fluorescent dye with a "rhodamine-like" structure was studied in both liquid media and adsorbed onto a photo-active substrate, TiO_2 . Regarding the liquid samples, it was found that the highest fluorescent quantum yield and fluorescence lifetimes was obtained in a solution of dichloromethane, whereas larger Stokes shifts were found in acetonitrile and ethanol, pointing out to the presence of ICT mechanisms as the main deactivation pathways, in these solvents. The triplet–triplet absorption spectra were also monitored, in acetonitrile, showing a huge band in the range of 350–580 nm, in an argon purged sample. When adsorbed onto the photoactive material, the molecule presented some interesting features, the most important one being the generation of the dye radical cation, after photoexcitation, indicating the injection of electrons into the conduction band of the semiconductor. The photodegradation kinetics of the dye- TiO_2 system was investigated, by enabling both the self-photosensitized pathway and the photocatalytic mechanism, reaching to a 3-fold increase in the photocatalytic capability, when compared with the non-photoactive substrate, cellulose. By means of laser flash photolysis, the powdered dye- TiO_2 sample was monitored and it was found that, in the presence of the dye, there was an electron–hole recombination that made the characteristic band of h^+ to disappear, whereas an excessive population of entrapped e^- could be observed, when compared with the pure TiO_2 nanopowder. Ultimately, the work reflects the photochemical characterization of a new organic fluorescent NIR dye which possesses a huge capability to interact with the TiO_2 photoactive substrate, in the presence of light, although its stability still offers some drawbacks when concerning future usage in photovoltaic and photochemical applications.

Acknowledgements

Thanks are due to FCT (Portugal's Foundation for Science and Technology), for the funding projects ERA-MNT/0003/2009 and Pest-OE/CTM/LA0024/2013 and for the PhD fellowships (SFRH/BD/95358/2013 and SFRH/BD/95359/2013) of David S. Conceição and Diana P. Ferreira, respectively.

References

- Mulders JLL, Steenhuysen LWG. The performance of dyes and dye mixtures of rhodamine 6G/rhodamine 560 and of styryl 8/styryl 9 for single mode cw ring laser operation. *Opt Commun* 1985;54(5):295–8.
- Faraggi M, Peretz P, Rosenthal I, Weinraub D. Solution properties of dye lasers. Rhodamine B in alcohols. *Chem Phys Lett* 1984;103(4):310–4.
- Reisfeld R, Grinberg M, Levchenko V, Kukliński B, Mahlik S, Magdassi S, et al. Sol–gel glasses with enhanced luminescence of laser dye Rhodamine B due to plasmonic coupling by copper nanoparticles. *Opt Mater* 2014;36(10):1611–5.
- Zehentbauer FM, Moretto C, Stephen R, Thevar T, Gilchrist JR, Pokrajac D, et al. Fluorescence spectroscopy of Rhodamine 6G: concentration and solvent effects. *Spectrochim Acta Part A Mol Biomol Spectrosc* 2014;121:147–51.
- Barigelletti F. Effect of temperature on the photophysics of rhodamine 101 in a polar solvent. *Chem Phys Lett* 1987;140(6):603–6.
- Conceição DS, Ferreira DP, Vieira Ferreira LF. Photochemistry and cytotoxicity evaluation of heptamethinecyanine near infrared (NIR) dyes. *Int J Mol Sci* 2013;14(9):18557.
- Conceição DS, Ferreira DP, Graça VC, Silva CR, Santos PF, Vieira Ferreira LF. Photochemical studies of new benzothiazole- and benzoselenazole-derived aminosquarylium dyes. *Tetrahedron* 2015;71(6):967–76.
- Chen C, Qi X, Zhou B. Photosensitization of colloidal TiO_2 with a cyanine dye. *J Photochem Photobiol A Chem* 1997;109(2):155–8.
- Long J, Liu X, Guo H, Zhao B, Tan S. Effect of conjugated side groups on the photovoltaic performances of triphenylamine-based dyes sensitized solar cells. *Dyes Pigments* 2016;124:222–31.
- Ye S, Kathiravan A, Hayashi H, Tong Y, Infahsaeng Y, Chabera P, et al. Role of adsorption structures of Zn-Porphyrin on TiO_2 in dye-sensitized solar cells studied by sum frequency generation vibrational spectroscopy and ultrafast spectroscopy. *J Phys Chem C* 2013;117(12):6066–80.
- Tsai H-HG, Tan C-J, Tseng W-H. Electron transfer of squaraine-derived dyes adsorbed on TiO_2 clusters in dye-sensitized solar cells: a density functional theory investigation. *J Phys Chem C* 2015;119(9):4431–43.
- Wu T, Liu G, Zhao J, Hidaka H, Serpone N. Photoassisted degradation of dye Pollutants. V. Self-Photosensitized oxidative transformation of rhodamine B under visible light irradiation in aqueous TiO_2 dispersions. *J Phys Chem B* 1998;102(30):5845–51.
- Chen F, Zhao J, Hidaka H. Highly selective deethylation of rhodamine B: adsorption and photooxidation pathways of the dye on the $\text{TiO}_2/\text{SiO}_2$ composite photocatalyst. *Int J Photoenergy* 2003;5(4).
- Tseng D-H, Juang L-C, Huang H-H. Effect of oxygen and hydrogen peroxide on the photocatalytic degradation of monochlorobenzene in aqueous suspension. *Int J Photoenergy* 2012;2012:9.
- Chu L, Anastasio C. Formation of hydroxyl radical from the photolysis of frozen hydrogen peroxide. *J Phys Chem A* 2005;109(28):6264–71.
- Tamaki Y, Furube A, Katoh R, Murai M, Hara K, Arakawa H, et al. Trapping dynamics of electrons and holes in a nanocrystalline TiO_2 film revealed by femtosecond visible/near-infrared transient absorption spectroscopy. *Comptes Rendus Chim* 2006;9(2):268–74.
- Tojo S, Tachikawa T, Fujitsuka M, Majima T. Direct observation of one-electron oxidation processes of aromatic sulfides in TiO_2 colloidal solution by laser flash photolysis. *Phys Chem Chem Phys* 2004;6(5):960–4.
- Furube A, Asahi T, Masuhara H, Yamashita H, Anpo M. Charge carrier dynamics of standard TiO_2 catalysts revealed by femtosecond diffuse reflectance spectroscopy. *J Phys Chem B* 1999;103(16):3120–7.
- Ferreira DP, Conceição DS, Prostota Y, Santos PF, Vieira Ferreira LF. Fluorescent "rhodamine-like" hemicyanines derived from the 6-(N,N-diethylamino)-1,2,3,4-tetrahydroxanthylum system. *Dyes Pigments* 2015;112:73–80.
- Tian Z, Tian B, Zhang J. Short communication. *Dyes Pigments* 2013;99(3):1132–6.
- Vieira Ferreira LF, Ferreira Machado IL. Surface Photochemistry: organic molecules within nanocavities of calixarenes. *Curr Drug Discov Technol* 2007;4(4):229–45.
- Vieira Ferreira LF, Costa SMB. Fluorescence quantum yield evaluation of strongly absorbing dye solutions as a function of the dye concentration. *J Luminescence* 1991;48:395–9.
- Botelho do Rego AM, Vieira Ferreira LF. 4. Photonic and electronic spectroscopies for the characterization of organic surfaces and organic molecules adsorbed on surfaces. In: Hari Singh N, editor. *Experimental methods in the physical sciences*. Academic Press; 2001. p. 269–354.
- Ferreira DP, Conceicao DS, Ferreira VRA, Graça VC, Santos PF, Vieira Ferreira LF. Photochemical properties of squarylium cyanine dyes. *Photochem Photobiol Sci* 2013;12(11):1948–59.

- [25] Prostota YA. Convenient method for synthesis of 6-(N,N-Diethylamino)-9-(2-carboxyphenyl)-1,2,3,4-tetrahydroxanthylum perchlorate. *Chem Heterocycl Compd* 2004;40(1):116–7.
- [26] Prostota Y, Kachkovsky OD, Reis LV, Santos PF. New unsymmetrical squaraine dyes derived from imidazo[1,5-*a*]pyridine. *Dyes Pigments* 2013;96(2):554–62.
- [27] Hinckley DA, Seybold PG, Borris DP. Solvatochromism and thermochromism of rhodamine solutions. *Spectrochim Acta Part A Mol Spectrosc* 1986;42(6):747–54.
- [28] Tian Z, Tian B, Zhang J. Synthesis and characterization of new rhodamine dyes with large Stokes shift. *Dyes Pigments* 2013;99(3):1132–6.
- [29] Folli A, Pochard I, Nonat A, Jakobsen UH, Shepherd AM, Macphee DE. Engineering photocatalytic cements: understanding TiO₂ surface chemistry to control and modulate photocatalytic performances. *J Am Ceram Soc* 2010;93(10):3360–9.
- [30] Beaumont PC, Johnson DG, Parsons BJ. Excited state and free radical properties of rhodamine dyes in aqueous solution: a laser flash photolysis and pulse radiolysis study. *J Photochem Photobiol A Chem* 1997;107(1–3):175–83.
- [31] Beaumont PC, Johnson DG, Parsons BJ. Photophysical properties of laser dyes: picosecond laser flash photolysis studies of Rhodamine 6G, Rhodamine B and Rhodamine 101. *J Chem Soc Faraday Trans* 1993;89(23):4185–91.
- [32] Schneider J, Matsuoka M, Takeuchi M, Zhang J, Horiuchi Y, Anpo M, et al. Understanding TiO₂ Photocatalysis: mechanisms and materials. *Chem Rev* 2014;114(19):9919–86.
- [33] Jing L, Zhou J, Durrant JR, Tang J, Liu D, Fu H. Dynamics of photogenerated charges in the phosphate modified TiO₂ and the enhanced activity for photoelectrochemical water splitting. *Energy Environ Sci* 2012;5(4):6552–8.
- [34] Tachikawa T, Tojo S, Kawai K, Endo M, Fujitsuka M, Ohno T, et al. Photocatalytic oxidation reactivity of holes in the sulfur- and carbon-doped TiO₂ powders studied by time-resolved diffuse reflectance spectroscopy. *J Phys Chem B* 2004;108(50):19299–306.
- [35] Wilkinson F, Willsher CJ, Uhl S, Honnen W, Oelkrug D. Optical detection of a photoinduced thermal transient in titanium dioxide powder by diffuse reflectance laser flash photolysis. *J Photochem* 1986;33(3):273–8.